Structure of Smectic Defect Cores: X-Ray Study of 8CB Liquid Crystal Ultrathin Films

Jean-Philippe Michel, Emmanuelle Lacaze,* and Michel Goldmann

INSP, Universités Paris 6 et 7, UMR-CNRS 7588, Campus Boucicaut, 140 rue de Lourmel, F-75015 Paris, France

Marc Gailhanou

LURE, Batiment 209D, Universit Paris Sud, F-91405 Orsay CEDEX, France

Marc de Boissieu

LTPCM, INPG, BP 75, 38402 Saint Martin d'Hères, France

Michel Alba

LLB, UMR12 CEA-CNRS, CEA-Saclay, F-91191 Gif-sur-Yvette CEDEX, France

We study the structure of very thin liquid crystal films frustrated by antagonistic anchorings in the smectic phase. In a cylindrical geometry, the structure is dominated by the defects for film thicknesses smaller than 150 nm and the detailed topology of the defects' cores can be revealed by x-ray diffraction. They appear to be split in half tube-shaped rotating grain boundaries (RGB). We determine the RGB spatial extension and evaluate its energy per unit length. Both are significantly larger than the ones usually proposed in the literature.

The combined technological interest for liquid crystal (LC) devices and for small size devices now requires a precise understanding of the microscopic structure of LC films. Progress in the LC physics is often intimately connected to the understanding of the LC defects [1]. If now the LC defects are precisely described from a macroscopic point of view, a microscopic description is still lacking, with only simulations [2] currently available. The use of powerful techniques such as x-ray diffraction performed with synchrotron radiation sources allows us now to bridge such a gap. In lamellar phases (e.g., smectic phases in thermotropic systems), the most common defects are focal conics. They are singularity lines where the layer curvature is not defined and around which the layers rotate. They are ellipses (degenerated into straight lines, the disclinations, in "oily streaks") conjugated with hyperbolas (degenerated into curvature walls, in oily streaks) [1,3,4]. The inner structure of these singularity lines remains unknown since they are buried within the deformed film and only a very small amount of matter is involved. To overcome this first problem, we have studied very thin smectic films in which the defects dominate the film structure. In this limit, the defects can no longer be considered as singularity lines but are split into two-dimensional structures. We have used oriented samples of oily streaks, self-assembled in regular stripes, and we have performed x-ray diffraction experiments at synchrotron sources that allowed us to determine the rotation of the layers close to the defects. We have revealed the topological structure of the disclination core. The spatial extension has been determined and the energy per unit length estimated. Both values are at least 1 order of magnitude larger than the usual estimations proposed in the literature.

We have studied 8CB (4-*n*-octyl-4′-cyanobiphenyl) smectic films adsorbed on a MoS_2 substrate, deformed through strong antagonistic anchorings at both interfaces but ordered by the single crystal surface of MoS_2 (molybdenum disulfide). The relaxation of the constraints imposed by the antagonistic anchorings occurs through the formation of oily streaks associated with a periodic network of flattened hemicylinders, parallel to the substrate [5]. These hemicylinders are associated with half disclinations locked on the substrate at the centers of curvature of the quarters of cylinders (points *D* in Fig. 1), conjugated with curvature walls.

The 8CB, smectic in bulk at 25 °C, is used without any further purification (BDH-Germany). A 0.1 mol/l solution of 8CB in dichloromethane is deposited on a freshly cleaved surface of MoS_2. The film's thickness, *e*, is controlled by spin coating at a speed varying between 1000 and 6000 rpm. The film thickness is checked by optical microscopy and determined by the film color, according to the Newton tint table, with an average error of 15 nm in the 70–350 nm range. The sample is annealed at 80 °C to allow the formation of an ordered $8CB/MoS_2$ interface which imposes a strong planar unidirectional anchoring within large domains [6], antagonistic to the homeotropic anchoring at the 8CB/air interface.

X-ray diffraction experiments are performed on the D2AM (ESRF, Grenoble, France) and H10 (LURE, Orsay, France) synchrotron beam lines. The photon's energy is fixed at 8 keV, the beam spot is 50×50 μm^2 large. We take advantage of the periodic character of the smectic *A* phase and detect the first Bragg peak associated with the 8CB bulk period ($q_s = 0.198$ Å^{-1}). In our resolution limited setup, after geometrical corrections (the background is
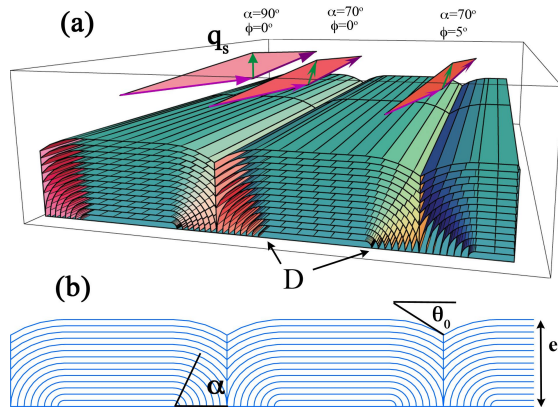
FIG. 1 (color online).   (a) Scheme of layers, concentrically stacked into flattened hemicylinders lying flat on the substrate, with half disclinations located at points D. Examples of diffusion triangles for various α and ϕ angles are drawn, with enhanced incident angles for clarity, and momentum transfer, $\vec{q}_s$, indicated, perpendicular to the substrate for ($\alpha = 90°$, $\phi = 0°$). (b) Flattened hemicylinders, presented in the plane perpendicular to the hemicylinder axes: The curvature walls between neighboring hemicylinders are characterized by the angle at the top, denoted by θ_0. The layers' director orientation is associated with the α angle.

FIG. 2 (color online).   Bragg intensity profile with ϕ for different α values ($e = 200$ nm). The narrowing at small α values reveals a weaker mosaicity and is related to the strong anchoring on the substrate.

subtracted; the evolution of the beam footprint and of the penetration depth leading to a transmission factor step are taken into account [5]), the Bragg intensity is proportional to the number of layers oriented with the director parallel to the wave vector, $\vec{q}_s$. The orientation of the layers is then followed by tilting $\vec{q}_s$ and measuring the evolution of the Bragg intensity. The ϕ angle is defined as the angle between the diffraction plane and the hemicylinder axes. The α angle is defined in the plane perpendicular to the hemicylinder axes as the disorientation of $\vec{q}_s$ and such as the disorientation of the layers' director, with respect to the substrate surface [Fig. 1(b)]. We have first checked that the cylindrical symmetry imposed by the anchoring antagonism is preserved within the smectic film whatever the e values: The ϕ scans of the Bragg intensity remain centered at $\phi = 0$, whatever the α values (see Fig. 2 for $e = 200$ nm). We have then measured the Bragg intensity as a function of α for $\phi = 0$, $\alpha = 0°$ corresponding to the layers perpendicular to the substrate and $\alpha = 90°$ corresponding to the layers parallel to it. Figure 3 presents the evolution when e decreases from 450 to 70 nm. All curves are normalized with respect to the integrated intensity for $0° \leq \alpha \leq 85°$. Thus the main frame presents the distribution of rotating layers between $\alpha = 0°$ and $\alpha = 85°$, for $e = 200$, 150, and 70 nm. The null intensity from $\alpha = 0°$ to $\alpha = 7°$ is associated with the 8CB critical angle ($\theta_{8CB} = 0.17°$). When α becomes smaller than $7°$, the incident beam tilt angle becomes smaller than θ_{8CB} and the beam penetration becomes negligible. The rapid increase at $85°$ corresponds to the layers parallel to the substrate and is present for all e values. In the inset, the
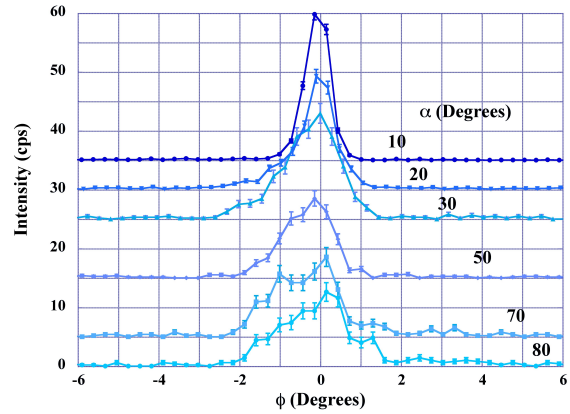
quasiconstant Bragg intensity, for $e = 450$ nm, illustrates that, for a thick film, only the signal of the bulk organized in flattened hemicylinders is detected, associated with a quasiconstant distribution of rotating layers from $\alpha = 0°$ to $\alpha = 85°$ [5]. The pronounced evolution of the distribution shape as e decreases discloses the increasing influence of the half-disclination inner structure: The number of rotating layers appears larger at small α than at large α. For very small thicknesses ($e = 70$ nm), the x-ray signal is controlled by the half-disclination structure, leading to Bragg intensity detected only for $7° \leq \alpha \leq 25°$ and at $\alpha = 90°$. If $e \geq 150$ nm, layers rotating up to $\alpha = 85°$ are measured, indicating that the half-disclination size is smaller than 150 nm. The negligible half-disclination con-
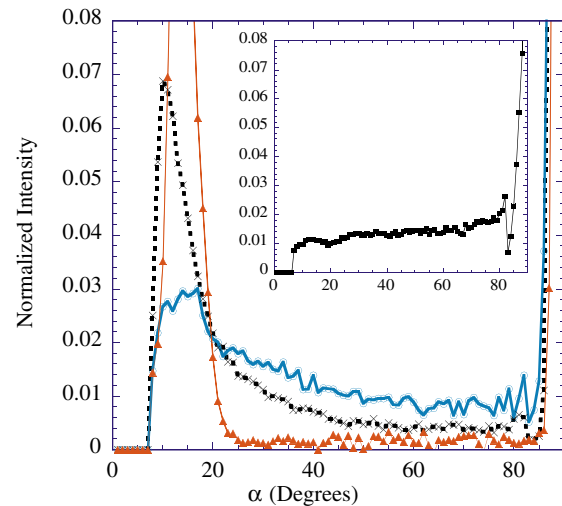

FIG. 3 (color online).   Corrected Bragg intensity variation with α. The intensity is normalized with respect to the integrated intensity from $0° \leq \alpha \leq 85°$. Curves for thin films are shown in the main frame [$e = 70$, 150, and 200 nm (full triangles, crosses, and open circles, respectively)] and for a thicker film in the inset [$e = 450$ nm (full squares)].

tribution to the x-ray data, if $e = 450$ nm, indicates that its size does not vary significantly with the thickness.

The gap observed in 70 nm thick films, between flat layers ($\alpha = 90°$) and rotating ones ($7° \leq \alpha \leq 25°$), associated with the still preserved cylindrical symmetry of the film, allows us to model the split mode of the half disclination by a rotating grain boundary (RGB). This RGB partitions the parallel layers from the rotating ones [Fig. 4(a)] and indeed eliminates a larger number of rotating layers at high α values than at low α ones.

In order to extract the RGB shape from the x-ray data, we define $r(\alpha)$ as the polar coordinate of the RGB, taken from the center of curvature, O, of the quarter cylinder [Fig. 4(b)]. Taking into account the curvature walls between the quarters cylinders, characterized by the upper θ_0 angle, defined in Fig. 1(b), the number of layers in the film, $n(\alpha)$, rotating from α to $\alpha + 1°$ is evaluated:

$$n(\alpha) \propto \frac{e \sin\theta_0}{\cos\alpha} - r(\alpha) \quad \text{for } \alpha \leq 90° - \theta_0;$$
$$\propto e - r(\alpha) \quad \text{for } \alpha \geq 90° - \theta_0. \tag{1}$$

The number of layers is also proportional to $i(\alpha)$, the x-ray intensity. The observed high intensity at small α in Fig. 3 shows that the RGB spatial extension in the direction associated with α close to $0°$ is negligible and the proportionality between $n(\alpha)$ and $i(\alpha)$ is obtained, using a small α_0 value, however, higher than $7°$: $n(\alpha_0) \propto (e \frac{\sin\theta_0}{\cos\alpha_0}) \approx A i(\alpha_0)$, leading to

$$r(\alpha) = e \frac{\sin(\theta_0)}{\cos(\alpha_0)} \left(\frac{\cos(\alpha_0)}{\cos(\alpha)} - \frac{i(\alpha)}{i(\alpha_0)} \right); \quad \alpha \leq 90° - \theta_0$$
$$= e \left(1 - \frac{i(\alpha) \sin(\theta_0)}{i(\alpha_0) \cos(\alpha_0)} \right); \quad \alpha \geq 90° - \theta_0. \tag{2}$$

We have to estimate now the characteristic θ_0 angle. The observed quasiconstant evolution of x-ray data between $\alpha = 50°$ and $\alpha = 85°$ suggests that $\theta_0 \gtrsim 40°$ for 150 nm $\leq e \leq 200$ nm. Postulating a value $\theta_0 = 60°$, two similar profiles of the RGB are obtained [Fig. 4(b)] for $e = 200$ nm and $e = 150$ nm, as expected. These profiles have been extrapolated continuously between $\alpha = 7°$ and $\alpha = 0°$ down to the O point. They are only slightly modified, when varying the θ_0 value between $\theta_0 = 90°$ and $\theta_0 = 40°$.

The contribution of this RGB profile to the x-ray intensity can now be calculated, using the reverse procedure. It is found negligible for $e = 450$ nm, in agreement with the experimental results. On the contrary, the evolution towards ultrathin films is driven by the RGB presence. The geometry of films thinner than 80 nm can be deduced from the profile of Fig. 4(b). They are composed of flat layers alternating with quasiperpendicular ones, in agreement with the x-ray results on the 70 nm thick film. It should be noted that these high disorientations are present what-
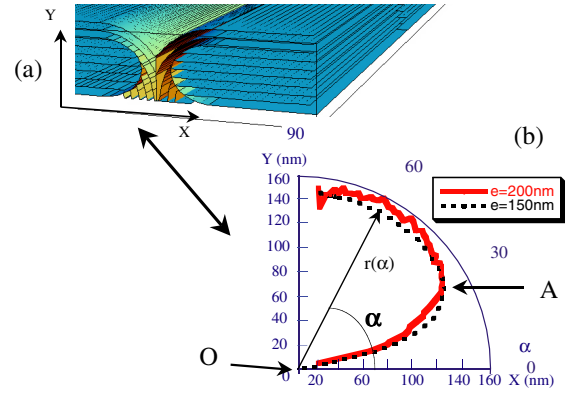

FIG. 4 (color online). (a) Scheme of enlarged flattened hemicylinders close to the half disclinations. The arrow associates a schematized half-disclination split in RGB with the profile extracted from the x-ray data. (b) RGB profile, extracted from the x-ray data in cases of thicknesses 150 nm (dotted line) and 200 nm (solid line) and a value $\theta_0 = 60°$, presented in the plane perpendicular to the hemicylinder axes.

ever the film thickness, since they always exist at the bottom of the buried defects.

The RGB can be described as a half tube with a quasielliptical cross section of minor axis 140 nm and semimajor axis 110 nm [deduced from Fig. 4(b)]. Such a spatial extension is significantly larger than λ, the smectic penetration length, equal to some nanometers, the distance usually associated with the focal conic cores in the literature. The origin of focal conic cores is related to the replacement of elastic curvature by dilation. A split mode in grain boundaries, characterized by local dilation of the layers, should then be a general property of focal conics. Such a replacement should be independent of the film thickness, as experimentally observed, and it should be independent of the anchoring energy values at the interfaces. It should mainly depend on the ratio between the elastic and compression modulus and on the disorientations imposed by the external constraints [7], leading to large spatial extensions, similarly for focal conics of different systems.

However, one expects the width of the RGB to be of the order of λ. An exact value of the width cannot be obtained through x-ray measurements and depends on the detailed structure of the RGB. The RGB is definitely not a simple grain boundary because it cannot account for the topological continuity of the layers, contrary to straight curvature walls [7,8]. Indeed, from point O to point A of the RGB [see Fig. 4(b)], 20 flat layers have to accommodate 45 rotating layers. This necessitates 20 dislocations between the start of the RGB (point O) and point A, as well as between point A and the other RGB extremity. The simplest models for the RGB correspond either to a grain boundary with many dislocations (even if they are not detected though x-ray diffraction or optical microscopy measurements [9]) or to a nematic envelope along the RGB [10]. Following these

two assumptions, the energy per unit length of the RGB can be calculated and associated with the half-disclination core energy.

In the dislocation hypothesis, this energy is calculated using the energy of a simple grain boundary [8], increased by 40 times the dislocation energy term, of the order of K_{8CB} [3] ($K_{8CB} = 11 \times 10^{-12}$ Jm^{-1} being the smectic 8CB curvature modulus [11]):

$$E_{RGB} = 40K_{8CB} + 1/2 \int_0^{\pi/2} \frac{K}{\lambda} r(\alpha) \frac{\cos(\frac{\pi}{2} - \alpha)}{2}$$
$$\times [\tan(\pi/2 - \alpha)/2 - (\pi/2 - \alpha)/2]d\alpha$$
$$= 42K_{8CB}, \tag{3}$$

leading to an energy per unit length mainly imposed by the dislocations energy.

In the hypothesis of a nematic envelope, the RGB energy can also be estimated, considering that the nematic envelope replaces a smectic envelope whose order parameter is equal to the smectic bulk order parameter:

$$E_{RGB} = P_{RGB}\left(\frac{a}{2}\Psi^2(T_0 - T)^s - \frac{b}{4}\Psi^4\right)\delta$$
$$= P_{RGB}[a^2(T - T_0)^{2s}/4b]\delta = 108K_{8CB}, \tag{4}$$

where $P_{RGB} = 350$ nm is the RGB perimeter, δ is the thickness envelope taken as equal to 1 nm, Ψ is the smectic order parameter, T_0 the transition temperature ($T_0 = 33.5\,°C$), a and b are the second- and fourth-order coefficients, s is the critical exponent in the de Gennes free energy versus Ψ and temperature ($a^2/b = 3.3 \times 10^6$ J K$^{-0.68}$ m^{-3}, $s = 0.34$ [12]).

These two simple evaluations of the RGB energy per unit length are of the same order of magnitude (42–108*K). Improved approximations would call for a finer description of the RGB structure. In the first model, the dislocation distribution along the RGB should be taken into account and, in the second model, a continuous evolution of the smectic order parameter [13]. These calculations demonstrate that the energy per unit length is at least 1 order of magnitude higher than K, the elastic modulus, whereas a value of the order of K is usually proposed in the literature for the focal conic core energy per unit length [14–16]. On the contrary, this result is consistent with a value of 15*K [8], indirectly obtained from the observations of toroidal focal conics in a lamellar/sponge system. Both results suggest then that the disclination and focal conic core energy per unit length are closer to 10–100*K than to K, the exact value depending on the geometry of the different systems.

X-ray measurements of thin smectic films deformed through a 90° antagonism of anchoring at both interfaces have revealed the structure of half-disclination cores. They appear to be split in half-tubed RGB, with a spatial extension of 140×110 nm^2 and an energy per unit length between 40*K and 110*K, K being the elastic modulus.

Both values are more than 1 order of magnitude higher than the values usually proposed in the literature. As for focal conics, the half-disclination structure is imposed by the replacement of elastic curvature by dilation. In the case of similar ratios between compression and elastic modulus, different systems submitted to high disorientations should also present split modes of the cores in grain boundaries of large spatial extensions. The high energy per unit length is due to the topological discontinuity of the layers from either part of the RGB. This discontinuity can be accounted for either by a grain boundary with a high density of dislocations or by the presence of a nematic envelope. Such high energies per unit length could constitute a general feature of focal conics and disclinations, because only straight grain boundaries allow topological connections between the layers. Our results not only can be generalized to different defects of lamellar phases (for example, one can think of copolymer or amphiphilic systems that are of fundamental and technological importance in many applications) but also demonstrate the ability of x-ray diffraction to probe soft matter fine structures. It is now possible, using synchrotron radiation sources, to reveal the detailed inner structure of defects, buried into smectic films.

---

*Electronic address: emmanuelle.lacaze@insp.jussieu.fr

[1] G. Friedel, Ann. Phys. (Paris) **18**, 273 (1922).

[2] S. Mkaddem and E. C. Gartland, Phys. Rev. E **62**, 6694 (2000).

[3] M. Kléman, *Introduction to Liquid Crystals* (Les Éditions de Physique, Paris, 1977).

[4] M. Kléman, O. D. Lavrentovich, and Yu. A. Nastishin, *Dislocation and Disclination in Mesomorphic Phases*, Dislocation in Solids Vol. 12 (Elsevier, New York, 2004).

[5] J. P. Michel, E. Lacaze, M. Alba, M. de Boissieu, M. Gailhanou, and M. Goldmann, Phys. Rev. E **70**, 011709 (2004).

[6] E. Lacaze, J. P. Michel, M. Goldmann, M. de Boissieu, M. Gailhanou, and M. Alba, Phys. Rev. E **69**, 041705 (2004).

[7] C. E. Williams and M. Kléman, J. Phys. (Paris), Colloq. **36**, C1-315 (1975).

[8] C. Blanc and M. Kléman, Eur. Phys. J. B **10**, 53 (1999).

[9] M. Ambrozic, S. Kralj, and S. Žumer, Eur. Phys. J. E **8**, 413 (2002).

[10] I. Dozov and G. Durand, Europhys. Lett. **28**, 25 (1994).

[11] M. J. Bradshaw, E. P. Raynes, J. D. Bunning, and T. E. Faber, J. Phys. (Paris) **46**, 1513 (1985).

[12] J. Thoen, H. Marynissen, and W. Van Dael, Phys. Rev. A **26**, 2886 (1982).

[13] S. Kralj and T. J. Sluckin, Phys. Rev. E **48**, R3244 (1993).

[14] P. G. de Gennes, C.R. Acad. Sci. Paris **275**, 549 (1972).

[15] Z. Li and O. D. Lavrentovich, Phys. Rev. Lett. **73**, 280 (1994).

[16] M. Kléman and O. D. Lavrentovich, Eur. Phys. J. E **2**, 47 (2000).